Fast high-temperature consolidation a novel way to understand the microstructural heterogeneities in nano-reinforced ferritic steels

X. Boulnat, D. Fabregue, M. Perez, S. Cazottes, Y. de Carlan

Proceedings of ICAPP 2015
May 03-06, 2015 - Nice (France)
Paper 15567

FAST HIGH-TEMPERATURE CONSOLIDATION: A NOVEL WAY TO UNDERSTAND THE MICROSTRUCTURAL HETEROGENEITIES IN NANO-REINFORCED FERRITIC STEELS

X. Boulnat[a,b,c], D. Fabrègue[b], M. Perez[b], S. Cazottes[b], Y. de Carlan[a]

[a] *CEA, DEN, Service de Recherches Métallurgiques Appliquées, 91191 Gif-sur-Yvette – France*
[b] *Université de Lyon, INSA-Lyon, MATEIS UMR CNRS 5510, 69621 Villeurbanne - France*
[c] *AREVA NP, Réacteurs et Services, Rue Alphonse Poitevin - Saint Marcel 71328 - France (current position)*

Tel: +33649142278
mail: xavier.boulnat@areva.com

Abstract – *Oxide-Dispersion Strengthened (ODS) ferritic steels were produced by powder metallurgy using a field-assisted sintering technique called spark plasma sintering (SPS). A multiscale characterization using electron microscopy combined with an in situ synchrotron X-Ray Diffraction allowed to understand the evolution of the heterogeneous microstructure. The influence of oxides precipitation was quantified by nanoscale observations to explain the microstructure heterogeneities in ferritic ODS alloys.*

I. INTRODUCTION

These last years, a co-operative international endeavor called Generation IV International Forum was organized to develop new concepts of competitive nuclear reactors that aim at optimizing the resources and minimizing the resulting wastes. Among the options for the construction of a fourth generation fast neutron reactor, the concept of Sodium-cooled Fast Reactor (SFR) is the most advanced system in France thanks to a large feedback. Making reactors competitive requires for the cladding tubes demanding specifications in terms of irradiation dose and temperature. The irradiation damage can create numerous defects in metallic materials that will result in significant swelling of the tubes. Since the design targets a minimum liquid sodium fraction and thus a configuration where fuel pins are close to each other, the dimensional variation of the in-service cladding tubes must be limited. Face-centered cubic (fcc) austenitic steels, well-known to exhibit excellent creep behavior, were however observed to drastically swell under irradiation dose higher than 100 to 130 dpa. To face this potential issue, the austenitic steels formerly used in SFRs may be replaced by base-centered cubic (bcc) ferritic/martensitic steels, which demonstrate much higher resistance to swelling.

Since ferritic steels exhibit moderate resistance to thermal creep compared to austenitic steels, new ferritic steels reinforced by oxides particles were designed to improve these properties. Due to their high creep strength and excellent swelling resistance, ferritic/martensitic oxide-dispersion strengthened (ODS) steels are thus serious candidates for tube cladding materials and are widely studied [1-6]. Their processing route involves powder metallurgy with powder milling and further high-temperature consolidation and extrusion. The whole fabrication is therefore complex and makes the microstructure evolution study not straightforward. Recent development led to two main options for ODS steel design: (i) 9-12Cr ODS ferritic/martensitic steels are easily workable. Thanks to the ferrite-to-austenite phase transformation, the anisotropic cold-worked microstructure can be conveniently transformed into a novel isotropic recrystallized microstructure. (ii) 14Cr ODS fully ferritic steels consist of an excellent alternative because their high chromium content enhances the corrosion resistance. Yet, their microstructure is much tougher to tailor since no allotropic transformation can be used. Specially, ODS ferritic steels exhibit abnormal grain growth leading to a microstructure with both very fine (submicronic) and very large (D > 10 μm) grains. This is also accompanied with an extraordinary resistance to recrystallization up to very high temperature (1300°C). The choice between transformable 9Cr or fully ferritic 14Cr ODS steels will be governed by the best compromise between fabrication and in-service performance, which has not been determined yet. Hence, every technological means must be investigated to assess the production of ODS steels. In order to study technological and metallurgical issues as well, a simpler method to produce model alloys to characterize would be interesting.

In this context, Spark Plasma Sintering (SPS) was considered. SPS is a pressure and electric field-assisted

consolidation technique that allows the powder to be directly heated up by a high-current intensity. Combined with sufficient hydrostatic pressure, this would allow to significantly reduce the overall consolidation time and thus obtain dense and homogeneous materials.

II. MATERIALS AND METHODS

II.A. Materials

A powder of high-Chromium ferritic steel was produced by ingot gas atomization by Aubert&Duval. The powder particles were then mechanically alloyed with submicronic yttria powder (Y_2O_3) using a high-energy attritor by Plansee SE. Milling conditions and microscopic evaluation of the as-milled powder are recalled in [7-8]. Using Focused Ion Beam (FIB) cross-sectioning of powder particles, the nanostructure was investigated by scanning electron microscopy (SEM) and Electron Back Scatter Diffraction (EBSD) [7]. Most of the grains were highly deformed and the smallest nanosized grains were not indexed due to a huge amount of dislocations, roughly estimated by Kernel Average Misorientation as over 10^{16} m^{-2}.

The chemical composition of the milled powder was measured by electron probe microanalysis and is reported in Table 1. This powder is representative of common industrial nanocrystalline powder widely used to process nanostructured materials. In this particular alloy, yttrium, titanium and oxygen are expected to form nanoparticles during hot processing.

Table 1 Chemical composition of the milled powder

Element (wt%)	Fe	Cr	W	Si	Mn	Y	O	Ti
Milled Powder	Bal.	14.5	1.01	0.3	0.3	0.16	0.15	0.32

II.B. Consolidation cycles

The possible consolidation steps are either hot isostatic pressing or spark plasma sintering for the isotropic processes, and hot extrusion for the anisotropic process. All involve non-isothermal cycles, with a heating ramp with a rate varying from few degrees per minute for HIPing to 500 degrees per minute for SPS. Then, a soaking step at maximum temperature is applied, usually at 1100°C for few minutes for SPS up to few hours for HIPing (Fig. 1). Here, SPS cycles were performed at two different soaking temperatures (850 and 1150°C) at a constant dwell time set at 5 minutes. SPS apparatus was HP D 25 of FCT Systeme GmbH equipped with graphite die and punches. SPS compacts were cylindrical with a diameter of 20 mm diameter and a height of 6 mm at a laboratory scale. In order to compare with more conventional process, HIPing was performed at 1150°C for 3 hours.

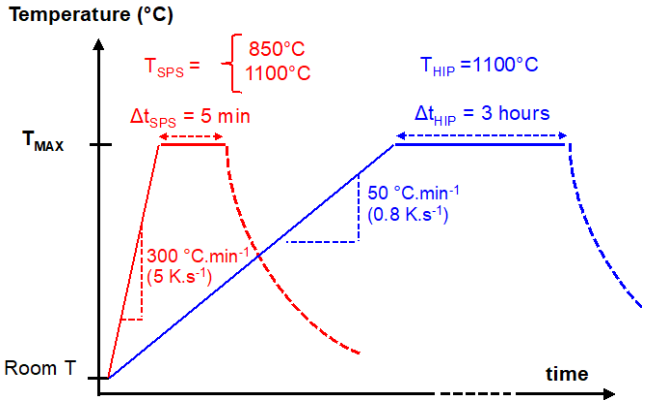

Fig. 1. Non-isothermal treatments by SPS and HIP

II.A. Characterization Methods

Grains were characterized by a scanning electron microscope (SEM) Zeiss Supra 55 VP with field-emis- sion gun (FEG) associated with an electron backscatter diffraction (EBSD) Oxford system for orientation and grain size measurement. Acquisition step size ranged from 20 to 80 nm with a tension of 15 kV.

Transmission Electron Microscopy (TEM) was performed on an apparatus TEM JEOL 2010F equipped with an Energy Dispersive X-Ray Spectroscopy (EDX) XMAX 80 for chemical analysis.

Atom Probe Tomography samples were prepared using a FEI Helios microscope equipped with a Focused Ion Beam, and APT analyses were made on a IMAGO LEAP 3000XHR, with laser or electric pulses. Analyses were performed at 50K, with a pulse fraction of 20% and a pulse rate of 200 Hz.

III. EXPERIMENTAL RESULTS

III.A Microstructure after consolidation

Fig. 2 illustrates the evolution of the microstructure as a function of the consolidation cycle. The microstructure of the compact SPSed at 850 °C is composed of isotropic grains from 50 nm to around 1 µm for the largest ones, which is very close to what was observed on the as-milled powder. At this state, the structure is composed of ultra-fine grained zones where subgrains of same or close orientation are surrounded by LAGB. Hence, primary recrystallization of new nuclei is not observed at this temperature. When considering the grain structure of the sample SPSed at higher temperatures (1150 °C), there is no specific crystallographic texture. The large grains do not seem to be more likely new nuclei with random orientation and have high-angle grain boundaries (>15°).

min

(b) SPS 1100°C – 5 min

(c) HIP 1100°C – 3 hours

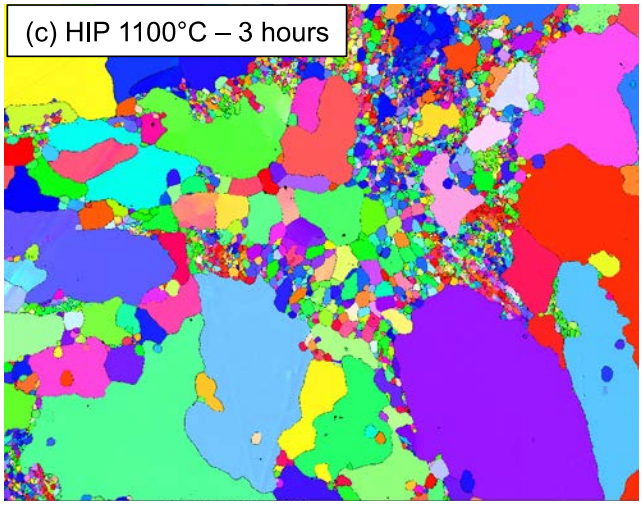

Fig. 2 Microstructure (grain orientation map) determined by EBSD of ODS steels consolidated by (a) SPS at 850°C, (b) SPS at 1150°C and (c) HIP at 1150°C. Bimodal microstructures are obtained at 1150°C after both SPS and HIP

Even if the SPS cycle is much faster than the HIP cycle, heterogeneous microstructures with coarse grains combined with nanostructured grains are obtained after both consolidation types. This limited effect of consolidation kinetics on grain growth mechanism leads to the conclusion that abnormal grains appear very rapidly at elevated temperature.

This critical temperature has thus been determined by *in situ* X-Ray diffraction. The peak diffraction broadening theory was used to determine the grain size and the dislocation density of the milled powder during non-isothermal treatment up to 1100°C, which is the typical consolidation temperature. The method for complete data analysis to calculate the grain size is reported in [10]. What is remarkable is that the abnormal grains can reach their critical size in a few seconds, once the critical temperature for abnormal growth (around 900°C) is reached. This explains why SPS at elevated temperature, which is above 900°C, cannot avoid the appearance of bimodal microstructure.

The bimodal microstructure is highly related to the grain boundary mobility, and especially how the grain boundaries are pinned by second-phase particles. Therefore, the grain growth kinetics may be linked to the precipitation kinetics, that is the formation of oxides in steels during consolidation. Thus, the precipitation state was carefully studied in the samples consolidated by SPS.

III.B. Precipitation of oxides in consolidated materials

After consolidation treatments, the resulting precipitation states were characterized by transmission electron microscopy (TEM) and Atom-probe Tomography (APT). Nanosized particles are visible in ultrafine grains after SPS at 850°C (not shown here). This is consistent with Small-Angle Neutron Scattering investigations that highlighted the formation of nanoparticles at this temperature [9]. After SPS at 1100°C, nanoparticles and coarser particles are observed as well (Fig. 3). The ‘coarse’ precipitates (diameter up to 100 nm) were identified by TEM Energy Dispersive X-Ray spectroscopy (EDX) as titanium-rich oxides. Fine particles were detected all over the grains by High-Resolution TEM (HRTEM) or in two-beam conditions (Fig. 4). Indeed, the coherent character of the particles makes it difficult to visualize these nanoscale precipitates in conventional mode. When observing in two-beam mode, the misfit between precipitates and matrix generates so-called Moiré fringes [11].

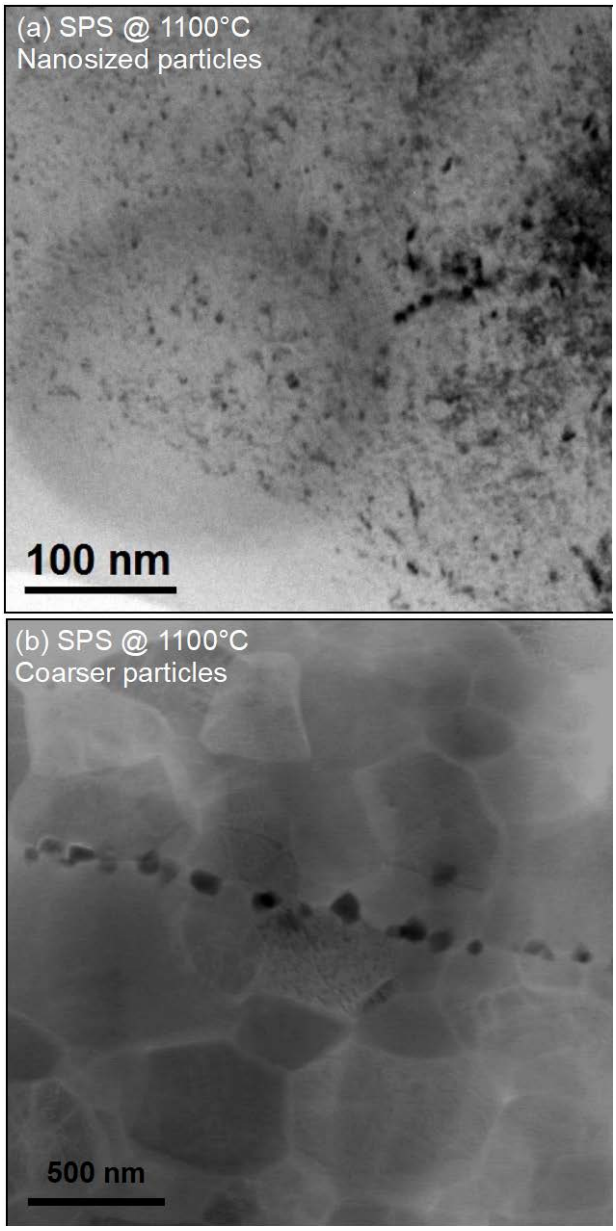

Fig. 3 Bright field TEM image of nanoparticles in a coarse grain after SPS at 1100°C.

Both coherent Y_2O_3 and $Y_2Ti_2O_7$ were identified. Cuboidal fcc precipitates were evidenced presenting the following Orientation relationship with the matrix:

{100}Fe || {100}fcc and <100>Fe || <100> fcc

,fcc being $Y_2Ti_2O_7$ or Y_2O_3 . The precipitates observed and the orientation relationship (OR) found are in agreement with what was previously observed by Ribis and de Carlan [11] in an ODS steel extruded at 1100°C and then annealed at 1100°C. Three types of precipitates were detected in this sample:

(i) $Y_2Ti_2O_7$-type pyrochlore oxide with a fcc structure ;

(ii) Y_2O_3-type yttria oxide with a bcc structure ;
(iii) Y2O3 with a fcc structure

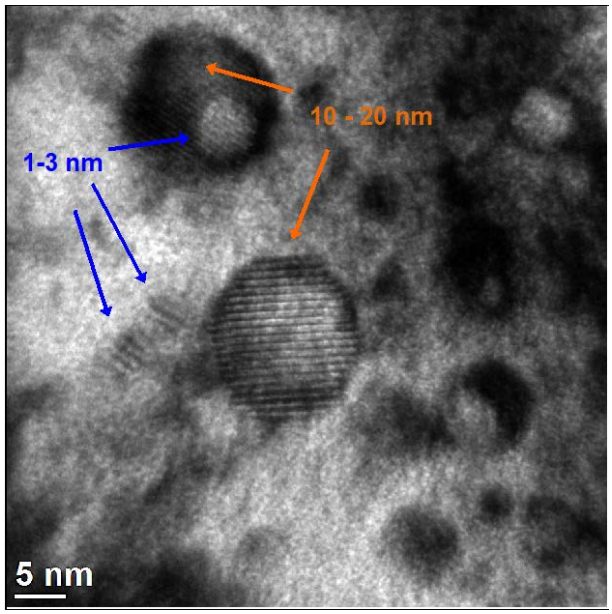

Fig. 4 Nanoparticles observed by High-resolution TEM on Sample after SPS at 1100°C.

To complete the precipitation characterization, atom-probe tomography was used to determine whether yttrium and titanium were present in the particles. As highlighted in Fig. 5, the clustering of yttrium and titanium is effective after SPS at 1100°C. This is consistent with the identification of the nanosized oxides by TEM.

These particles can efficiently pin the grain boundaries of selected grains, hence reducing their mobility even at high temperature. The pining effect can occur within the first minutes of consolidation, since precipitation occurred very rapidly during SPS. Since these particles are very stable during heat treatment [9,11], the pinning effect can induce the microstructure thermal stability at high temperature. This is why, even after HIPing for 3 hours, the bimodal microstructure is still present.

A complete scenario, to explain the occurrence of abnormal growth is proposed in [7]. Based on the calculation of the stored energy at each step of the consolidation process, the appearance of this structure is explained by the initial heterogeneous spatial distribution of stored energy due to high-energy attrition of the MA powder. The plastic work due to milling is the cause of the so-called abnormal growth. The heterogeneous microstructure is then stabilised by the nano-precipitation described above.

V. CONCLUSIONS

To conclude, experimental insights were brought to understand the microstructure evolution of ODS ferritic steels. A multiscale characterization using Electron Backscatter Diffraction and Transmission Electron Microscopy was performed after consolidation, providing substantial insight into the grain growth mechanisms.

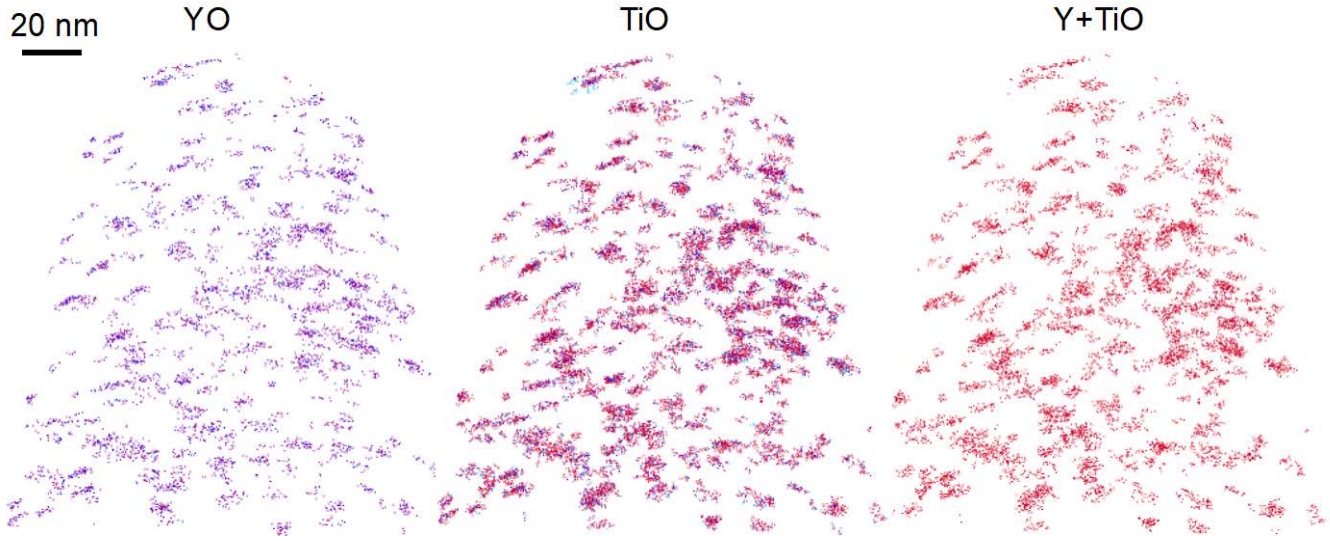

Fig. 5 Reconstruction map of yttrium, titanium and oxygen ions in the probed tip from sample SPS at 1100°C.

The resulting grain structure was observed to be heterogeneous with both ultra-fine grains and much larger grains. *In situ* Synchrotron X-Ray Diffraction experiments have been performed to reveal the microstructural evolution process leading to the bimodal grain structure of ODS ferritic steels. This demonstrated that abnormal structure could appear in a few seconds at typical consolidation temperature (1100°C).An accurate analysis of the microstructure evolution, associated to stored energy calculations, allowed to proposed a scenario to explain the specific ODS microstructure.

ACKNOWLEDGMENTS

This work was made in the frame of a tripartite agreement between the CEA, AREVA NP, and EDF and also in the MATTER project, which received funding from the European Commission within the 7th Framework Programme under grant agreement number 269706.

REFERENCES

[1] S. UKAI, M. HARADA, H. OKADA, M. INOUE, S. NOMURA, S. SHIKAKURA, T. NISHIDA, M. FUJIWARA, K. ASABE, J. Nucl. Mater. 204 (1993) 74.

[2] S. UKAI, M. FUJIWARA, J. Nucl. Mater. 307–311 (2002) 749.

[3] R.L. KLUEH, D.S. GELLES, S. JITSUKAWA, A. KIMURA, G.R. ODETTE, B. VAN DER SCHAAF, J. Nucl. Mater. 307–311 (2002) 455.

[4] P. DUBUISSON, Y. DE CARLAN, V. GARAT, M. BLAT, J. Nucl. Mater. 428 (2012) 6.

[5] S. SAROJA, A. DASGUPTA, R. DIVAKAR, S. RAJU, E. MOHANDAS, M. VIJAYALAKSHMI, K.B.S. RAO, B. RAJ, J. Nucl. Mater. 409 (2011) 131.

[6] M.A. AUGER, V. DE CASTRO, T. LEGUEY, A. MUÑOZ, R. PAREJA, J. Nucl. Mater. 436 (2013) 68.

[7] X. BOULNAT, D. FABRÈGUE, M. PEREZ, S. URVOY, D. HAMON, Y. DE CARLAN, Powder Metallurgy, 2014, Vol. 57, Issue 3, pp. 204-211

[8] X. BOULNAT, D. FABRÈGUE, M. PEREZ, M-H. MATHON, Y. DE CARLAN, Metallurgical and Materials Transactions A, 2013, Vol. 44, Issue 6, pp. 2461-2465

[9] X. BOULNAT, M. PEREZ, D. FABRÈGUE, T. DOUILLARD, M-H. MATHON, Y. DE CARLAN, Metallurgical and Materials Transactions A, 2014, Vol. 45, Issue 3, pp. 1485-1497

[10] N. SALLEZ, X. BOULNAT, A. BORBÉLY, J.L. BÉCHADE, Y. DE CARLAN, C. MOCUTA, D. FABRÈGUE, M. PEREZ, Y. BRÉCHET, Acta Materialia, Vol. 87, 2015, pp. 377–389.

[11] J. RIBIS and Y. DE CARLAN, Acta Materialia, Vol. 60, 2012, pp. 238 – 252.